Peptide-templating dye-sensitized solar cells

2010 Nanotechnology 21 185601

(http://iopscience.iop.org/0957-4484/21/18/185601)

Nanotechnology **21** (2010) 185601 (6pp) doi:10.1088/0957-4484/21/18/185601

Peptide-templating dye-sensitized solar cells

Tae Hee Han[1], Hyoung-Seok Moon[1], Jin Ok Hwang[1], Sang Il Seok[2], Sang Hyuk Im[2,3] and Sang Ouk Kim[1,3]

[1] Department of Materials Science and Engineering, Korea Advanced Institute of Science and Technology (KAIST), Daejeon 305-701, Republic of Korea
[2] KRICT-EPFL Global Research Laboratory, Advanced Materials Division, Korea Research Institute of Chemical Technology, Daejeon 305-600, Republic of Korea

E-mail: imromy@krict.re.kr and sangouk.kim@kaist.ac.kr

Received 21 December 2009, in final form 15 March 2010
Published 9 April 2010
Online at stacks.iop.org/Nano/21/185601

Abstract
A hollow TiO_2 nanoribbon network electrode for dye-sensitized solar cells (DSSC) was fabricated by a biotemplating process combining peptide self-assembly and atomic layer deposition (ALD). An aromatic peptide of diphenylalanine was assembled into a three-dimensional network consisting of highly entangled nanoribbons. A thin TiO_2 layer was deposited at the surface of the peptide template via the ALD process. After the pyrolysis of the peptide template, a highly entangled nanotubular TiO_2 framework was successfully prepared. Evolution of the crystal phase and crystallite size of the TiO_2 nanostructure was exploited by controlling the calcination temperature. Finally, the hollow TiO_2 nanoribbon network electrode was integrated into DSSC devices and their photochemical performances were investigated. Hollow TiO_2 nanoribbon-based DSSCs exhibited a power conversion efficiency of 3.8%, which is comparable to the conventional TiO_2 nanoparticle-based DSSCs (3.5%). Our approach offers a novel pathway for DSSCs consisting of TiO_2 electrodes via biotemplating.

(Some figures in this article are in colour only in the electronic version)

1. Introduction

Biotemplating exploits naturally generated biomolecular structures as templates for functional nanomaterials [1–3]. Unlike synthetic templating methods that usually require harsh processing conditions [4–6], biotemplating enables the construction of complicated hierarchical architectures through a mild, biocompatible process [7–10]. To date, several advanced device fabrications for photonic crystals [11], electronic circuits [12] and secondary rechargeable batteries [13] have been exploited, taking advantage of highly specific biomolecular interactions. Recently, we reported a biotemplating comprising peptide self-assembly of diphenylalanine and atomic layer deposition (ALD) [9]. Diphenylalanine is a well-known structural motif for the β-amyloid associated with Alzheimer's disease (figure 1(a)) [7]. This aromatic peptide assembly exhibits remarkably high thermal stability and thus allows for further high temperature processing in conjunction with conventional vacuum deposition such as ALD [9]. The self-limiting ALD deposition of a thin TiO_2 layer [14–16] upon a highly entangled peptide nanoribbon xerogel and subsequent pyrolysis successfully generated highly entangled hollow TiO_2 nanoribbons with a large surface area.

Dye-sensitized solar cells (DSSCs) based on a hybrid of organic materials and inorganic nanoparticles are currently attracting widespread attention because of their potential for low cost and high-throughput manufacturing [17–22]. A standard DSSC consists of a TiO_2 nanoparticle photoanode film on transparent conducting oxide (TCO) glass, a monolayer light absorbing chromophore, a platinum-coated TCO glass counter electrode and an iodide electrolyte. Upon illumination, the photoexcited dye injects an electron into the conduction band of the TiO_2, which migrates through the TiO_2 nanoparticle through interparticular hopping and collects at the transparent electrode substrate. The light-sensitizing dye is subsequently regenerated electrochemically through an electrolyte, which is commonly based on an iodide/triiodide redox couple. Among diverse efforts for

[3] Authors to whom any correspondence should be addressed.

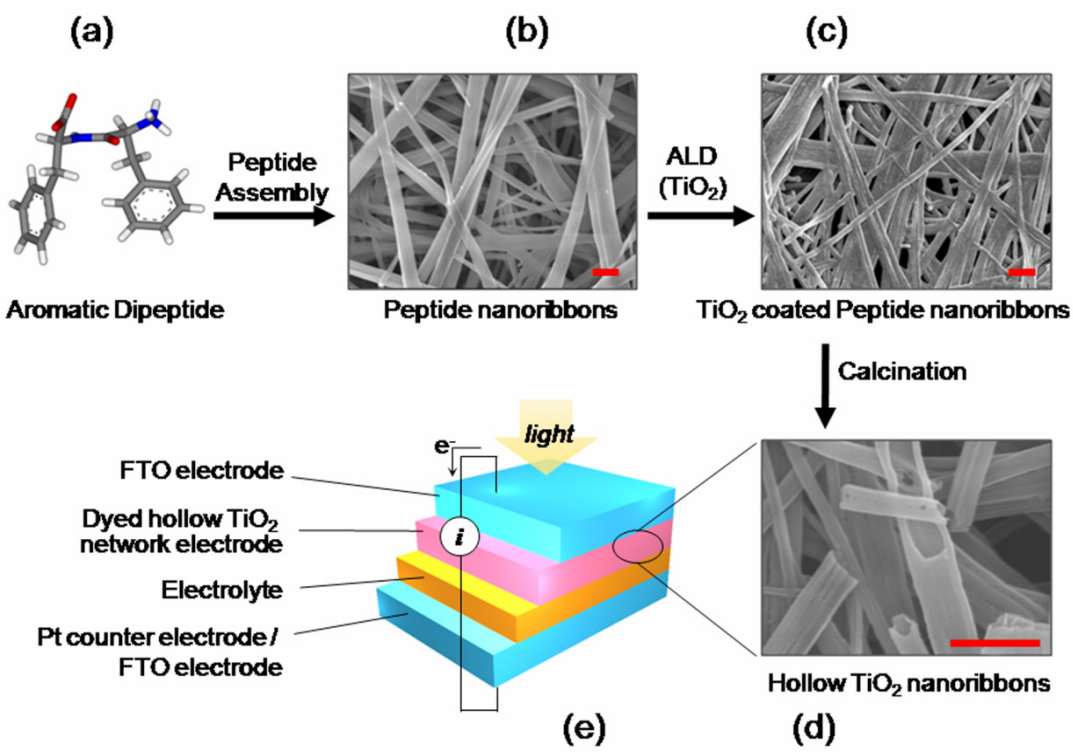

Figure 1. Schematically illustrated process for highly entangled hollow TiO_2 nanoribbons and DSSCs. (a) Molecular structure of diphenylalanine. (b) SEM image of 3D xerogel consisting of peptide nanoribbons. SEM images of the entangled TiO_2 nanoribbons (c) before and (d) after the calcination of the peptide template. (e) A cross section of DSSCs made from peptide-templating hollow TiO_2 nanoribbons. Scale bars: 1 μm.

high efficiency solar cells, much research has been done to improve the interfacial contact between TiO_2 nanoparticles through surface modification because the numerous junctions make surface traps and consequently recombine the generated charge carriers reducing the electron lifetime [21–27]. To overcome the disadvantage of nanocrystalline TiO_2 while keeping the surface area, tubular TiO_2 nanostructures are suggested and successfully demonstrated to elongate the charge carrier's lifetime by reduced junctions [23–26]. Here we demonstrate the DSSC devices prepared from a highly entangled hollow TiO_2 nanoribbon photoanode templating diphenylalanine assembly. The direct carrier transport through highly entangled one-dimensional electrode architectures ensures rapid collection of carriers generated throughout the device by reducing surface traps in the interfacial junction between TiO_2 nanoparticles [21–27]. Furthermore, the highly open architecture enables easy infiltration of viscous electrolytes and hole transfer materials into the photoelectrode layer, which is crucial for an effective regeneration of oxidized dyes [13, 26]. We investigated the evolution of the crystal phase and crystallite size in the TiO_2 nanostructures by controlling the heat treatment temperature and the corresponding performances of DSSCs. Our approach represents a unique pathway to prepare the hollow TiO_2 nanoribbon-based DSSCs which exhibited comparable power conversion efficiency with conventional nanoparticle-based DSSCs.

2. Experimental methods

2.1. Materials

A lyophilized form of diphenylalanine was purchased from Bachem (Switzerland) and used without further purification. Chloroform was purchased from Merck (Germany). Titanium tetra-isopropoxide (TTIP, $Ti(OC_3H_7)_4$) was purchased from Mecharonics (Korea) and used as received.

2.2. Fabrication of hollow TiO_2 nanoribbons

Peptide organogel was prepared by dissolving a predetermined amount of diphenylalanine into chloroform via sonication (concentration: 8 mg ml^{-1}) and subsequent cooling. Xerogel was prepared by spontaneous evaporation of chloroform at ambient temperature. A thin layer of TiO_2 was deposited on the xerogel by ALD (140 °C and 3 Torr). TTIP was used as a precursor and ammonia (NH_3) gas was used as a reactant. The TTIP was carried by an inert Ar gas stream. One deposition cycle of TiO_2 consisted of four steps: (i) deposition of the TTIP precursor, (ii) a purge pulse of Ar, (iii) an injection of reactive NH_3 gas and (iv) another purge pulse of Ar. The flow rates were 50 sccm for the Ar purge and 25 sccm for the NH_3 purge. During the deposition, 100 sccm of Ar gas was continuously supplied into the reactor as a carrier gas. Under these conditions, the saturated growth rate of the TiO_2 layer was ~0.2 Å $cycle^{-1}$. In a typical deposition process, 500 cycles were repeated to generate a film with a thickness of

10 nm. The peptide template was removed by calcination at 400 or 500 °C for 1 h under air.

2.3. Morphology characterization

The morphology of the peptide xerogel and TiO_2 nanoribbon framework was analyzed by a field emission scanning electron microscope (FESEM; Hitachi S-4800 SEM, Japan). A high-resolution transmission electron microscope (HRTEM; JEOL JEM-2100F, Japan) was used to characterize the crystalline morphology of the TiO_2 nanoribbons. The crystal structure of the nanoribbons was characterized by means of powder x-ray diffraction (XRD) with Cu Kα radiation ($\lambda = 1.5418$ Å) on a D/Max 2500 x-ray diffractometer (Rigaku, Japan).

2.4. Dye-sensitized solar cell assembly

0.13 g of TiO_2-coated peptide nanoribbons was dispersed in 10 ml ethanol by sonication and 0.26 g of PEG600 was added. The solution was placed in a convection oven at 70 °C for one day to evaporate the ethanol solvent. Finally, the well-dispersed paste of TiO_2-coated peptide nanoribbons was prepared by brief sonication. The paste was coated on the FTO glass (TEC15, USA) having a 50 nm TiO_2 blocking layer by a doctor blade coating. To remove the peptide nanoribbon template and transform the remaining amorphous TiO_2 layer into crystal, the coated paste was calcined at 400 or 500 °C. Upon thermal annealing, the temperature was gradually elevated to the annealing temperature during 1 h and maintained at the annealing temperature for 1 h and was then cooled down to room temperature. The calcined samples were then dipped into an absolute ethanol solution containing 0.5 mM *cis*-bis(isothiocyanato)bis(2,2′-bypyridi-4,4′-dicarboxylatoruthenium (II) bis-tetrabutylammonium) (Ru535-bisTBA, Solaronix: N719 dye) for 12 h. The Pt-coated counter electrode was prepared by dropping 5 mM of H_2PtCl_6 in *i*-propanol onto FTO glass and heating it up to 400 °C for 20 min. The cells were assembled by combining the dye-absorbed calcined hollow TiO_2 nanoribbons and Pt-coated counter electrodes using a thermal adhesive film (Surlyn, 60 μm, DuPont). A solution containing 0.60 M 1-butyl-3-methylimidazolium iodide (BMII, Merck), 0.03 M I_2 (Sigma-Aldrich), 0.1 M guanidin thiocyanate (Sigma-Aldrich) and 0.5 M 4-*tert*-butylpyridine (Aldrich) in the mixture of acetonitrile and valeronitrile with a volume ratio of 85:15 was used as the redox electrolyte. The electrolyte was injected by vacuum back-filling, prior to sealing the hole by a Surlyn film and a cover glass. In order to improve electrical contact, lead contact pads were made on both sides of the electrodes by using an ultrasonic soldering iron. The active area of the photoelectrode was found to be 0.18 cm^2. The conventional DSSCs consisting of commercial TiO_2 nanopowder (Degussa, P-25) were also prepared with the same thickness as hollow TiO_2 nanoribbon-based DSSC for comparison (annealing temperature: 500 °C, thickness: 3 μm).

2.5. Device performance of dye-sensitized solar cells

The photocurrent–voltage (I–V) characteristics of the cells were measured under illumination of 1 sun (AM 1.5 G, 100 mW cm^{-2}) with a solar simulator (Newport, Class A, 91195A) using a Keithley 2420 sourcemeter and calibrated Si-reference cell (certified by NREL). The incident photo-to-current conversion efficiency (IPCE) was measured by a fully computerized home-designed system comprising a light source (300 W Xe lamp, Newport, 66902) with a monochromator (Newport Cornerstone 260) and a multimeter (Keithley 2002).

3. Results and discussion

The preparation of a hollow TiO_2 nanoribbon electrode and the assembly of DSSCs are schematically described in figure 1. Firstly, peptide organogel was prepared by dissolving diphenylalanine in chloroform and forming opaque aggregates during cooling to room temperature. By evaporating the high volatile chloroform, xerogel was instantly prepared from the organogel under ambient conditions. Figure 1(b) shows an SEM image of the xerogel frameworks. Linear and flat nanoribbons were observed as the frameworks of the xerogel. The peptide framework was coated with a ∼10 nm thickness continuous TiO_2 layer by means of ALD. As shown in figure 1(c), the morphology that consisted of the highly entangled nanoribbons was well preserved during the ALD process performed at 140 °C. The peptide template was calcined at a high temperature such that the remaining TiO_2 network was composed of highly entangled hollow tubular nanoribbons. In this step, the crystalline structure varied depending on the calcination temperature. Figure 1(d) presents that the morphology of the peptide template was exactly replicated in the hollow TiO_2 nanoribbons. Figure 1(e) describes the schematic of the DSSCs fabricated in this work. The TiO_2 networks were applied as photoanodes in the configuration of DSSCs.

The nanoscale morphologies of hollow TiO_2 nanoribbons after pyrolysis at 400 °C and 500 °C are shown in figures 2(a) and (b), respectively. The SEM images confirm that TiO_2 nanoribbons have hollow tubular structures and are mutually connected to form a 3D network structure. Figures 2(c) and (d) show TEM images of isolated hollow TiO_2 nanoribbons obtained at 400 °C and 500 °C, respectively. The wall thicknesses of nanoribbons were confirmed to be approximately 10 nm and 21 nm, respectively. The nanoribbon's surface was smooth and uniform, confirming that the TiO_2 layer was uniformly deposited over the entire peptide template. The hollow TiO_2 nanoribbons were polycrystalline and their crystal domain size increased with annealing temperature.

The phase evolution and crystal structure of the TiO_2 nanoribbons were further characterized using powder XRD analysis (figure 2(e)). The thermal annealing at 400 °C led to a crystalline anatase TiO_2 (pattern (a)), while a higher temperature of 500 °C led to the nucleation of rutile phase (pattern (b)). At 400 °C, a broad peak at $2\theta = 25.3°$ which corresponds to the (101) plane diffraction of anatase TiO_2 (PDF no. 21-1272) was observed. The peak broadening was attributed to the small crystallite size and low crystallinity of the sample. Upon increasing the calcination temperature up to 500 °C, the intensities of anatase peaks increased. The width of

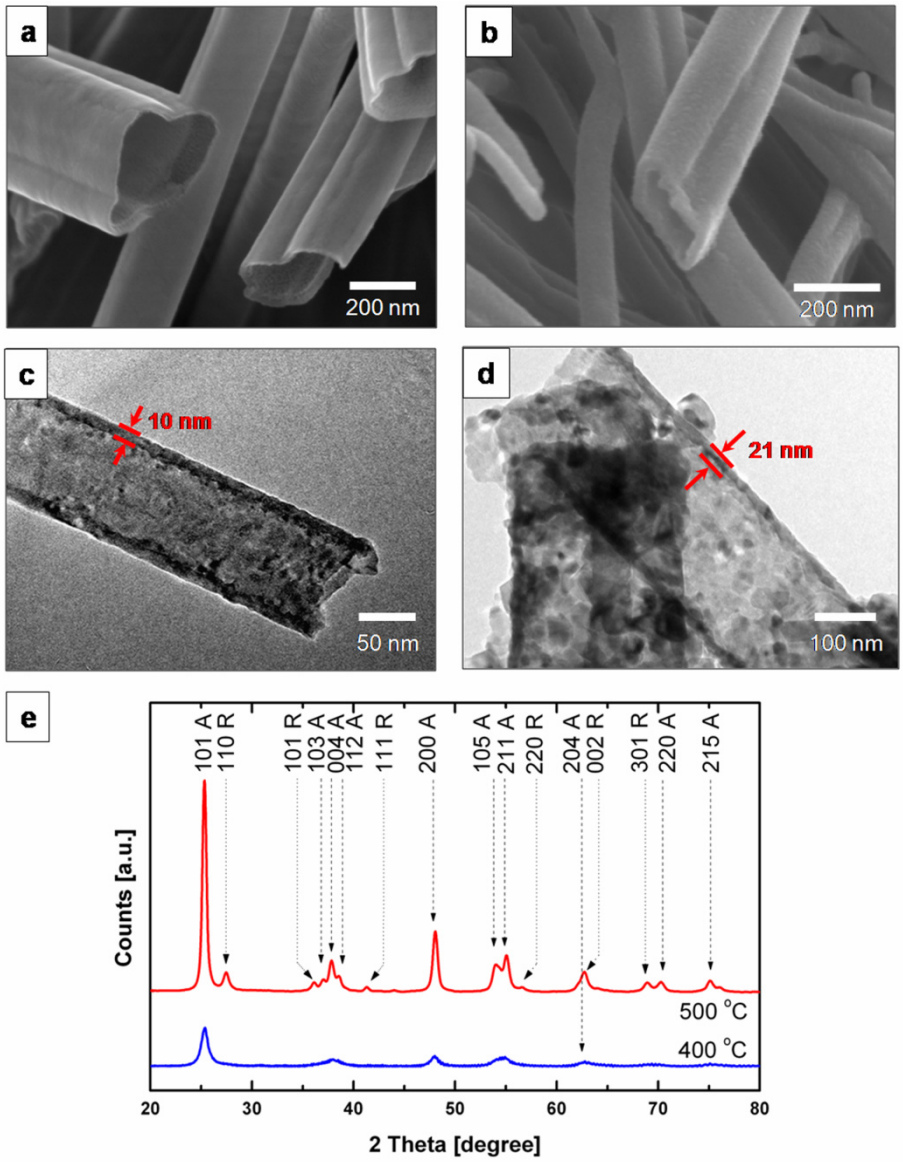

Figure 2. SEM and TEM images of hollow TiO_2 nanoribbons obtained by calcining at 400 °C ((a) and (c)) and 500 °C ((b) and (d)). (e) XRD patterns of hollow nanoribbons obtained by calcining at 400 °C and 500 °C, respectively.

the (101) plane diffraction peaks became narrower, due to the increase in anatase crystallite size (from 9.4 to 18.4 nm) (see table 1). An average crystallite size was calculated using the Scherrer equation:

$$L = \frac{0.9\lambda}{B(2\theta)\cos(\theta)} \tag{1}$$

where L is the crystallite size and $B(2\theta)$ is the linewidth. A calculated crystallite size was comparable to the wall thickness of hollow nanoribbons. Additionally, a small peak at $2\theta = 27.5°$, which corresponds to the (110) plane diffraction of rutile TiO_2 (PDF no. 21-1276), appeared. This indicates that the phase transformation from anatase to rutile was initiated. At this temperature, 7.9% of the anatase TiO_2 was transformed into rutile TiO_2. The crystallite size of rutile TiO_2 was evaluated as 14.4 nm. The phase composition of TiO_2 can be calculated from the integrated intensities of the anatase (101) and rutile (110) peaks according to the following equation [28]:

$$W_R = \frac{A_R}{0.886A_A + A_R} \tag{2}$$

where A_A and A_R represent the integrated intensity of the anatase (101) and rutile (110) peaks, respectively. At a higher temperature, the intensity of the anatase TiO_2 diffraction peak decreased significantly, whereas the intensity of the rutile TiO_2 diffraction increased, indicating that most of the anatase phase was transformed into the rutile phase. At 800 °C, the mass fraction of rutile reached 93.3% and the crystallite size of rutile TiO_2 was increased to 62.9 nm. The XRD results reveal that calcination at a high temperature induces not only the removal of peptide templates but also the growth of the crystallite and the subsequent phase transition.

In a typical device fabrication, the electrode substrate (fluorine-doped tin oxide (FTO) coated glass) was prepared

Table 1. Comparison of cell performances of DSSCs consisting of TiO_2 nanoribbons prepared at 400 and 500 °C and commercial TiO_2 nanoparticles (Degussa, P-25).

Calcination temperature (°C)	Phase content (%)	Crystal size (nm)	V_{oc} (V)	J_{sc} (mA cm^{-2})	FF (%)	η (%)	R_{shunt} (kΩ)	R_{series} (Ω)
400	(A) 100	9.4	0.68	5.5	65	2.4	3.26	76
500	(A) 92.1 (R) 7.9	(A)18.4 (R) 14.4	0.72	8.3	64	3.8	3.52	65
P-25	(A) 75 (R) 25	20	0.77	7.1	65	3.5	3.62	127

by depositing a thin blocking TiO_2 layer (50 nm in thickness) onto an FTO via spray pyrolysis. The TiO_2 layer played a role of adhesive between the titania nanoribbons and the substrate surface and prevented the direct contact of electrolyte with FTO. The 33.3 wt% of PEG600-based titania-coated peptide paste was then deposited on the substrate by a doctor blading. The deposited paste was calcined at 400 and 500 °C, respectively. We note that the FTO substrate was thermally damaged above 500 °C so that the devices were not prepared at higher temperature. The layer thickness of a hollow TiO_2 nanoribbon electrode was ∼3 μm. The resulting electrode was assembled into devices using standard approaches for DSSCs. The dye was adsorbed onto TiO_2 nanoribbons by immersing in an ethanol solution containing ruthenium complex photosensitizer. After injection of an electrolyte containing iodide mixture, platinized FTO glass was used as the counter electrode.

The IPCE spectra of hollow TiO_2 nanoribbon electrodes calcined at 400 °C and 500 °C are presented in figure 3(a). The IPCE can be expressed theoretically as the product of the light absorption efficiency of the dye, the quantum yield of electron injection and the efficiency of collecting the injected electrons at the conducting glass substrate [19, 22]. Both spectra show very similar spectral characteristics. The peak at 350 nm is contributed by the light absorption of TiO_2. The broad peak correlates to the sensitization of the dye. The overall IPCE of TiO_2 electrodes formed at 500 °C is approximately 1.6 times higher than that formed at 400 °C. The higher IPCE value of the TiO_2 electrode calcined at 500 °C is due to the larger crystallite size and packing density.

The photoelectrochemical characteristics of the dye-anchored TiO_2 electrodes were measured under simulated solar light irradiation (AM1.5, 100 mW cm^{-2}). Figure 3(b) shows the photocurrent–voltage (I–V) measurements of DSSCs comprising hollow TiO_2 nanoribbons obtained at 400 °C and 500 °C, respectively. The results show that the higher I_{sc} and open-circuit voltage (V_{oc}) were obtained in the DSSCs with the TiO_2 electrodes calcined at 500 °C. The solar cell parameters of the dye-anchored TiO_2-based solar cells were given in table 1. The device prepared with TiO_2 nanoribbons calcined at 400 °C exhibited an V_{oc} of 0.68 V, a short-circuit current density (J_{sc}) of 5.52 mA cm^{-2} and a fill factor (FF) of 65%, giving an overall power conversion efficiency (η) of 2.4%. Meanwhile, the device prepared with TiO_2 nanoribbons formed by calcining at 500 °C showed a V_{oc} of 0.72 V, a J_{ac} of 8.3 mA cm^{-2}, a fill factor of 64% and an efficiency of 3.8%. The J_{sc} increased with calcination

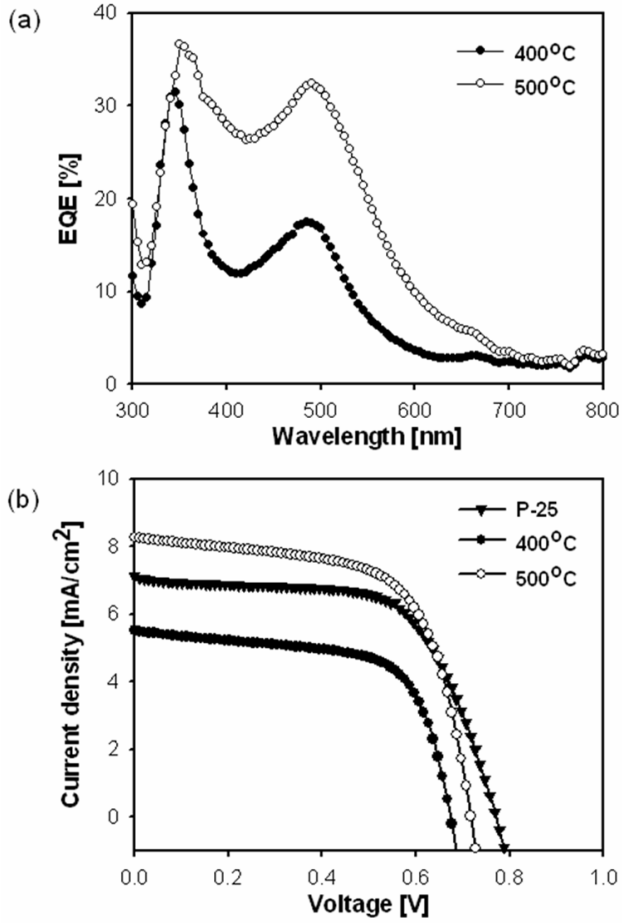

Figure 3. Characteristics of DSSCs. IPCE spectra (a) and photocurrent density–voltages curves (b) of TiO_2 nanoribbons calcined at 400 °C (filled circles) and 500 °C (unfilled circles), respectively. The device performance of commercial TiO_2 nanoparticle (Degussa, P-25)-based DSSCs is plotted for comparison.

temperature, which is attributed to the increase of IPCE (figure 3(a)). In the comparison of the device parameters of TiO_2 nanoribbons and conventional TiO_2 nanoparticle-based solar cells, the DSSC consisting of hollow TiO_2 nanoribbons showed a comparable efficiency with that (3.62%) of conventional DSSC of TiO_2 nanoparticles (P-25), which is a mixture of anatase and rutile (3:1). We note that the charge carrier's mobility is dominated by the junctions in nanocrystalline TiO_2-based DSSC [29, 30] even though the electron mobility of single-crystalline anatase is faster than that

of rutile [31, 32]. Likewise, in our experiments, inherently junction-modified hollow TiO_2 nanoribbons could improve the efficiency by reducing series resistance compared with conventional nanocrystalline TiO_2-based DSSC. We believe the J_{sc} and the power conversion efficiency could be further improved by the thickness control of hollow TiO_2 nanoribbons.

4. Conclusions

Hollow TiO_2 nanoribbon solar cell electrodes were successfully fabricated by a biotemplating method of peptide assembly and subsequent ALD. The crystalline structure of the resultant TiO_2 nanoribbons was investigated depending on the calcinating temperature of the peptide core template. While the low calcinating temperature of 400 °C generated pure anatase TiO_2 with a low crystallinity and small grain size, the high temperature of 500 °C created the mixed crystalline structure of rutile and anatase with an improved crystallinity and large grain size. The DSSC made from the mixed crystalline TiO_2 nanoribbon electrode revealed a better solar cell performance. The larger crystallite size of TiO_2 electrodes allowed the higher power conversion efficiency due to the reduced grain boundaries, and densely packed crystallites.

Acknowledgments

This work was supported by the National Research Laboratory Program (R0A-2008-000-20057-0), the Fundamental R&D Program for Core Technology of Materials, the World Class University (WCU) program (R32-2008-000-10051-0) and the Korea Foundation for International Cooperation of Science & Technology through the Global Research Laboratory (GRL) Program funded by the Korean government.

References

[1] Sotiropoulou S, Sierra-Sastre Y, Mark S S and Batt C A 2008 *Chem. Mater.* **20** 821
[2] Caruso R A 2004 *Angew. Chem. Int. Edn* **43** 2746
[3] Lee S M, Grass G, Kim G-M, Dresbach C, Zhang L, Gösele U and Knez M 2009 *Phys. Chem. Chem. Phys.* **11** 3608
[4] Shin D O, Kim B H, Kang J H, Jeong S-J, Park S H, Lee Y-H and Kim S O 2009 *Macromolecules* **42** 1189
[5] Park S H, Shin D O, Kim B H, Yoon D K, Kim K, Lee S Y, Oh S-H, Choi S-W, Jeon S C and Kim S O 2010 *Soft Matter* **6** 120
[6] Lee J, Orilall M C, Warren S C, Kamperman M, DiSalvo F J and Wiesner U 2008 *Nat. Mater.* **7** 222
[7] Reches M and Gazit E 2003 *Science* **300** 625
[8] Han T H, Kim J, Park J S, Park C B, Ihee H and Kim S O 2007 *Adv. Mater.* **19** 3924
[9] Han T H, Oh J K, Park J S, Kwon S-H, Kim S-W and Kim S O 2009 *J. Mater. Chem.* **19** 3512
[10] Han T H, Lee W J, Lee D H, Kim J E, Choi E Y and Kim S O 2009 *Adv. Mater.* doi:10.1002/adma.200903221
[11] Huang J, Wang X and Wang J L 2006 *Nano Lett.* **6** 2325
[12] Scheibel T, Parthasarathy R, Sawicki G, Lin X-M, Jeager H and Lindquist S L 2003 *Proc. Natl Acad. Sci. USA* **100** 4527
[13] Kim S-W, Han T H, Kim J, Gwon H, Moon H-S, Kang S-W, Kim S O and Kang K 2009 *ACS Nano* **3** 1085
[14] Knez M, Nielsh K and Niinistö L 2007 *Adv. Mater.* **19** 3425
[15] Kim J-Y, Kim J-H, Ahn J-H, Park P-K and Kang S W 2007 *J. Electrochem. Soc.* **154** H1008
[16] Shin H, Jeong D-K, Lee J, Sung M M and Kim J 2004 *Adv. Mater.* **16** 1197
[17] Hagfeldt A and Grätzel M 2000 *Acc. Chem. Res.* **33** 269
[18] Bach U, Lupo D, Comte P, Moser J E, Weissörtel F, Salbeck J, Spreitzer H and Grätzel M 1998 *Nature* **395** 583
[19] Grätzel M 2003 *J. Photochem. Photobiol.* **4** 145
[20] Lee K, Park S W, Ko M J, Kim K and Park N-G 2009 *Nat. Mater.* **8** 665
[21] Law M, Greene L E, Johnson J C, Saykally R and Yang P 2005 *Nat. Mater.* **4** 455
[22] Kang S H, Choi S-H, Kang M-S, Km J-Y, Kim H-S, Hyeon T and Sung Y-E 2008 *Adv. Mater.* **20** 54
[23] Varghese O K, Paulose M and Grimes C A 2009 *Nat. Nanotechnol.* **4** 592
[24] Zhu K, Vinzant T B, Neale N R and Frank A J 2007 *Nano Lett.* **7** 3739
[25] Kang T-S, Smith A P, Taylor B E and Durstock M F 2009 *Nano Lett.* **9** 601
[26] Mor G K, Shankar K, Paulose M, Varghese O K and Grimes C A 2006 *Nano Lett.* **6** 215
[27] Feng X, Shankar K, Varghese O K, Paulose M, Latempa T J and Grimes C A 2008 *Nano Lett.* **8** 3781
[28] Yu J, Su Y and Cheng B 2007 *Adv. Funct. Mater.* **17** 1984
[29] Van de Lagemaat J, Park N-G and Frank A J 2000 *J. Phys. Chem.* B **104** 2044
[30] Fisher A C, Peter L M, Ponomarev E A, Walker A B and Wijayantha K G U 2000 *J. Phys. Chem.* B **104** 949
[31] Nazeeruddin M K, Angelis F D, Fantacci S, Selloni A, Viscardi G, Liska P, Ito S, Takeru B and Grätzel M 2005 *J. Am. Chem. Soc.* **127** 16835
[32] Park N-G, van de Lagemaat J and Frank A J 2000 *J. Phys. Chem.* B **104** 8989